HPSTAR 064_2014

Lower critical field and SNS-Andreev spectroscopy of 122-arsenides: Evidence of nodeless superconducting gap

M. Abdel-Hafiez,[1,2,3,*] P. J. Pereira,[4] S. A. Kuzmichev,[5] T. E. Kuzmicheva,[6] V. M. Pudalov,[6,7] L. Harnagea,[8] A. A. Kordyuk,[9] A. V. Silhanek,[2] V. V. Moshchalkov,[4] B. Shen,[10] Hai-Hu Wen,[11] A. N. Vasiliev,[5,12] and Xiao-Jia Chen[1]

[1]*Center for High Pressure Science and Technology Advanced Research, 1690 Cailun Road, Shanghai 201203, China*

[2]*Département de Physique, Université de Liège, B-4000 Sart Tilman, Belgium*

[3]*Faculty of Science, Physics Department, Fayoum University, 63514 Fayoum, Egypt*

[4]*INPAC, Catholic University of Leuven, Celestijnenlaan 200D, B-3001 Leuven, Belgium*

[5]*Low Temperature Physics and Superconductivity Department, Physics Faculty, M. V. Lomonosov Moscow State University, 119991 Moscow, Russia*

[6]*P. N. Lebedev Physical Institute, Russian Academy of Sciences, Moscow 119991, Russia*

[7]*Moscow Institute of Physics and Technology, Moscow 141700, Russia*

[8]*Leibniz Institute for Solid State and Materials Research, IFW-Dresden, D-01171 Dresden, Germany*

[9]*Institute of Metal Physics of National Academy of Sciences of Ukraine, 03142 Kyiv, Ukraine*

[10]*Institute of Physics, Chinese Academy of Sciences, Beijing 100190, China*

[11]*National Laboratory for Solid State Microstructures and Department of Physics, Nanjing University, Nanjing 210093, China*

[12]*Theoretical Physics and Applied Mathematics Department, Ural Federal University, 620002 Ekaterinburg, Russia*

(Received 15 May 2014; revised manuscript received 21 August 2014; published 29 August 2014)

Using two experimental techniques, we studied single crystals of the 122-FeAs family with almost the same critical temperature, T_c. We investigated the temperature dependence of the lower critical field $H_{c1}(T)$ of a $Ca_{0.32}Na_{0.68}Fe_2As_2$ ($T_c \approx 34$ K) single crystal under static magnetic fields H parallel to the c axis. The temperature dependence of the London penetration depth can be described equally well either by a single anisotropic s-wave-like gap or by a two-gap model, while a d-wave approach cannot be used to fit the London penetration depth data. Intrinsic multiple Andreev reflection effect spectroscopy was used to detect bulk gap values in single crystals of the intimate compound $Ba_{0.65}K_{0.35}Fe_2As_2$, with the same T_c. We estimated the range of the large gap value $\Delta_L = 6$–8 meV (depending on small variation of T_c) and its a k space anisotropy of about 30%, and the small gap $\Delta_S \approx 1.7 \pm 0.3$ meV. This clearly indicates that the gap structure of our investigated systems more likely corresponds to a nodeless s-wave two gaps.

DOI: 10.1103/PhysRevB.90.054524 PACS number(s): 74.25.Bt, 74.25.Dw, 74.45.+c, 74.70.Xa

I. INTRODUCTION

Fe-based superconductors of the AFe_2As_2 type (122 system), where A is an alkaline-earth element (i.e., Ca, Ba, Sr), show an intermediate critical temperature T_c, high upper critical fields H_{c2} due to the small coherence lengths, and a low anisotropy ($\gamma \approx 2$) [1]. The identification of the symmetry and structure of the superconducting order parameter and the mechanism for Cooper pairing is of primary importance in Fe-based superconductors. Numerous efforts have been made since the discovery of high-T_c Fe-based superconductors to understand the physics of the pairing mechanism. It turns out that the physics of the pairing could be more complicated than originally thought, because of the multiband nature of low-energy electronic excitations [2]. In quasi-two-dimensional (2D) multiband superconductors two or more energy bands at the Fermi energy give rise to multiple energy gaps in the respective superconducting condensates [1,3–5]. Recent specific heat (C_P) and angle-resolved photoemission spectroscopy (ARPES) measurements provide clear evidence of multiple gap structures in the 122 system [6,7].

On the other hand, the density of states calculations show that the states at the Fermi level E_F are formed mainly by $3d$ electrons of Fe, thus the metallic-type conductance is mainly due to these $3d$ states [8,9]. This leads to the suggestion that any kind of spacer between FeAs blocks affects the level of doping rather than the fundamental pairing mechanism. Consequently, one could assume that spacer doping has a minor influence on the superconducting gap symmetry.

Various experimental data on the gap magnitude and anisotropy in k space are contradictory enough. In particular, C_P measurements are commonly used for gap quantification [7,10,11], though there are several known problems with data treatment. The C_P data contain a contribution from the lattice, which is subtracted to some extent in order to determine the electronic contribution. The lattice contribution to the C_P which is typically estimated by suppressing the superconducting transition, cannot be accurately obtained because of the very high upper critical field of the hole-doped and magnetic/structural phase transitions at higher temperatures of the parent compound. The majority of the earlier C_P data suffer from a residual low-temperature nonsuperconducting electronic contribution and show Schottky anomalies [10,12]. Moreover, superconductivity-induced electronic C_P is very sensitive to the sample quality and phase purity [11]. Also, in the earlier C_P data analysis, the data are commonly fitted to the phenomenological multiband model [13], which assumes a BCS temperature dependence of the gaps. However, our Andreev spectroscopy measurements [14–18] do not support this assumption and clearly show that the $\Delta(T)$ dependencies for the multiband superconductors (such as MgB_2 and

*m.mohamed@hpstar.ac.cn

Fe-based superconductors) deviate substantially from the BCS type because of the interband coupling. Finally, fitting the C_P data with the multiband model requires several adjustable parameters. It might therefore be that a combination of all the above obstacles causes dissimilar gap values (and, in particular, unrealistically large values, such as 11 and 3.5 meV [11]), obtained from the C_P measurements. In this context, it is very important to have the possibility of comparing the results obtained by two independent bulk, purely electronic probes; particularly good candidates are the the lower critical field, H_{c1}, and Andreev spectroscopy.

The determination of H_{c1}, the field at which vortices penetrate into the sample, allows one to extract the magnetic penetration depth λ, a fundamental parameter characterizing the superconducting condensate and carrying information about the underlying pairing mechanism. In the superconducting state, the temperature dependence of the penetration depth is a sensitive measure of low-energy quasiparticles, making it a powerful tool for probing the superconducting gap [19]. The lower critical field studies in LiFeAs [20,21], $Ba_{0.6}K_{0.4}Fe_2As_2$ [22], $Eu_{0.5}K_{0.5}Fe_2As_2$ [23], and FeSe [24] have supported the existence of two s-wave-like gaps. On the other hand, nodes in the SC gap have been reported in $NdFeAsO_{0.82}F_{0.18}$ and La-1111, where the magnetic penetration depth exhibited a nearly linear temperature dependence [25,26]. Also, a nodal pairing state of Sm-1111 has been suggested based on the T^2 dependence of the H_{c1} studies [27]. The interpretation of these results may also be impaired by substantial contributions from paramagnetic centers. In view of the existing divergence of conclusions about the gap symmetry derived from single-type measurements, there is a clear need to obtain a set of data by different techniques.

Although the superconducting order parameter has been investigated for similar compounds, i.e., $Ba_{0.65}Na_{0.35}Fe_2As_2$ [10] and $Ba_{0.68}K_{0.32}Fe_2As_2$ [11], its investigation in $Ca_{0.32}Na_{0.68}Fe_2As_2$ and $Ba_{0.65}K_{0.35}Fe_2As_2$ is necessary in order to further clarify the differences between these structurally similar systems. It has recently been shown, in Ref. [6], that $Ca_{0.32}Na_{0.68}Fe_2As_2$ is almost identical to the more studied $Ba_{0.65}K_{0.35}Fe_2As_2$ in terms of electronic band structure, Fermi surface topology, and superconducting gap distribution. Therefore we are able to combine here the results for these two compounds measured by different techniques. In this study we investigated whether both London penetration depth and intrinsic multiple Andreev reflection effect (IMARE) techniques may provide such conclusive and self-consistent information on the gap anisotropy. Based on our experimental data, we report on the superconducting gap properties of hole-doped $Ca_{0.32}Na_{0.68}Fe_2As_2$ and $Ba_{0.65}K_{0.35}Fe_2As_2$. Our analysis shows that the superconducting gaps determined through fitting to the London penetration depth for out-of-plane directions support two possible scenarios, namely, the presence of an anisotropic single gap and that of two s-wave-like gaps with different magnitudes and contributions. In addition, our IMARE spectroscopy of SNS-Andreev arrays formed by the break-junction technique for $Ba_{0.65}K_{0.35}Fe_2As_2$ reveals two nodeless gaps: a large gap, $\Delta_L = 6$–8 meV, with extended s-wave symmetry in k space, and a small gap, $\Delta_S = 1.7 \pm 0.3$ meV.

II. EXPERIMENTAL DETAILS

The dc magnetization measurements discussed in this paper were performed on a rectangular slab. Single crystals of $Ca_{0.32}Na_{0.68}Fe_2As_2$ were grown using NaAs as described in Ref. [28]. The chemical composition was verified by scanning electron microscope (SEM; Philips XL 30) equipped with an energy-dispersive x-ray spectroscopy probe. The magnetization measurements were performed using a superconducting quantum interference device magnetometer (MPMS-XL5) from Quantum Design. The good quality of the crystals was confirmed by various physical characterizations: (i) a sharp C_P anomaly associated with the superconducting phase transition is observed at 34 K [7]. (ii) The high value of the residual resistivity ratio is found to be $\rho_{(300\,\mathrm{K})}/\rho_{(36\,\mathrm{K})} = 12.8$ [7]. (iii) This system also stands out due to the absence of nesting between hole and electron pockets of the Fermi surface [6]. $Ba_{0.65}K_{0.35}Fe_2As_2$ single crystals were synthesized by the self-flux method using FeAs as the flux (for details see [29] and [30]). The chemical composition and crystal structure were checked by x-ray diffraction and energy-dispersive x-ray microanalysis. For both compounds a critical temperature $T_c \approx 34$ K is evidenced by magnetization measurements for $Ca_{0.32}Na_{0.68}Fe_2As_2$ and by Andreev spectra flatting in the case of the $Ba_{0.65}K_{0.35}Fe_2As_2$ study.

The single crystal prepared for Andreev spectroscopy studies is a thin plate of about $a \times b \times c = (2$–$4) \times (1$–$2) \times (0.05$–$0.15)\ \mathrm{mm}^3$. The crystal was attached to a spring sample holder by four liquid In-Ga pads (true four-contact connection), thus making the ab plane parallel to the sample holder, and then cooled down to $T = 4.2$ K. Next, the sample holder was curved mechanically ("break-junction" technique [31]). Under such deformation, the single crystal was cracked, generating superconductor–constriction (weak link)–superconductor (ScS) contact. Since the microcrack was located deep in the bulk of the sample and remote from current leads, the cryogenic clefts were free of overheating and degradation caused by impurity penetration, if any. The multiple Andreev reflection effect (MARE) is observed in ballistic constrictions of the metallic type, where the diameter $2a$ of the contact area is less than the quasiparticle mean free path l [32,33]. The MARE manifests itself causing an excess current at low biases in the current-voltage characteristic of ScS contact. With it, a series of dynamic conductance peculiarities called a subharmonic gap structure (SGS) appears. The position V_n of such peculiarities is determined by the superconducting gap, $V_n = 2\Delta/en$ (n, natural number) [34,35], at any temperature up to T_c [36,37]. For the high-transparency SnS-Andreev regime typical for our break-junction contacts, the supercurrent is absent, whereas the SGS represents dynamic conductance dips for the gap of both s- and d-wave symmetries [37,38]. The coexistence of two superconducting gaps would cause, obviously, two SGSs in the dI/dV spectrum.

Now we estimate the typical diameter of the contacts formed in the Ba-122 single crystals under study. The product of the normal-state bulk resistivity ρ_n and quasiparticle mean free path l was shown to be from $\rho_n l \approx 0.45 \times 10^{-9}\ \Omega \cdot \mathrm{cm}^2$ [39] to $\rho_n l \sim 1.7 \times 10^{9}\ \Omega \cdot \mathrm{cm}^2$ [40], determining the range of the experimental uncertainty. Taking the value of the in-plane bulk resistivity $\rho_n^{ab} \approx 0.4 \times 10^{-5}\ \Omega \cdot \mathrm{cm}$ for our Ba-122 single

crystal (as described in [41]) and the anisotropy value $\gamma^{H_{c2}} = \sqrt{\gamma^{\rho}} \approx 1.8$ [42], we determine the c-axis resistivity as $\rho_n^c \sim 1.3\times10^{-4}\ \Omega\cdot$cm. Hence, for $\rho_n l \approx 0.45\times10^{-9}\ \Omega\cdot\text{cm}^2$ [39] and for the Ba-122 samples used, the quasiparticle mean free path along the c direction is $l^c \approx 35$ nm. In the case of $\rho_n l \approx 1.7\times10^{-9}\ \Omega\cdot\text{cm}^2$ [40], one gets $l^c \approx 133$ nm. Finally, using the Sharvin formula for ballistic contact and the typical resistance of our SnS contact, $R = 10 \div 100\ \Omega$, we calculate the contact radius as $a = \sqrt{\frac{4}{3\pi}\frac{\rho_n l}{R}} = 13 \div 82$ nm. This rough estimation shows moderate superiority of l^c over a, thus proving the ballistic regime and allowing observation of one to three Andreev peculiarities in the dI/dV spectra [37].

Due to its layered structure, the Ba-122 single crystal cleaves along ab planes, with steps and terraces on cryogenic clefts. Each step is a natural stack of superconducting Fe-As blocks separated by metallic Ba spacers and, in fact, represents an S-n-S-n-$\cdots$-S array. In the ballistic mode, these arrays manifest themselves in the IMARE [43], which is similar to the intrinsic Josephson effect in cuprates [44]. In our experiment, after the sample cleavage the two superconducting banks slide over each other, touching at different terraces. By precise tuning of the sample holder one can probe tens of SnS contacts as well as arrays (containing various numbers of contacts) in order to check the reproducibility of the gap values. Since the S-n-S-n-$\cdots$-S stack contains a sequence of N connected junctions (with the transport along the c direction), the SGS dips appear at bias voltages that are N times higher,

$$V_n = \frac{2\Delta_i N}{en}; \tag{1}$$

so do other peculiarities caused by *bulk* properties of material. The number of junctions N could be determined by normalization of the spectrum of the array contact to that of single SnS contact; then the positions of each gap SGS should coincide. Probing such natural arrays, one obtains information about the true bulk properties of the sample (almost unaffected by surface states which seem to be significant in Ba-122 [45]) *locally* (within the contact size $a \approx$ 20–80 nm). This feature favors the accuracy increasing in gap magnitude measurements [46].

To get $dI(V)/dV$ spectra directly, we use a current generator that mixes dc with low-amplitude ac. In this way the standard modulation method is used. Narrow-band signal amplification with the help of a lock-in nanovoltmeter reveals dI/dV peculiarities even in the case of nearly flat $I(V)$ characteristics.

III. RESULTS AND DISCUSSION

A. Irreversible magnetization

Figure 1 (top) presents the field dependence of the isothermal magnetization M at various temperatures up to 45 kOe for $H \parallel c$. At $T = 2$ K, $M(H)$ exhibits irregular jumps close to $H = 0$, similarly to LiFeAs and $Ba_{0.65}Na_{0.35}Fe_2As_2$ superconductors [47,48]. These flux jumps are usually attributed to thermoelectromagnetic instabilities [49]. The inset in Fig. 1 (top) shows the temperature dependence of the magnetic susceptibility ($\chi = M/H$) measured by following zero-field-cooled procedures in an external field of 10 Oe

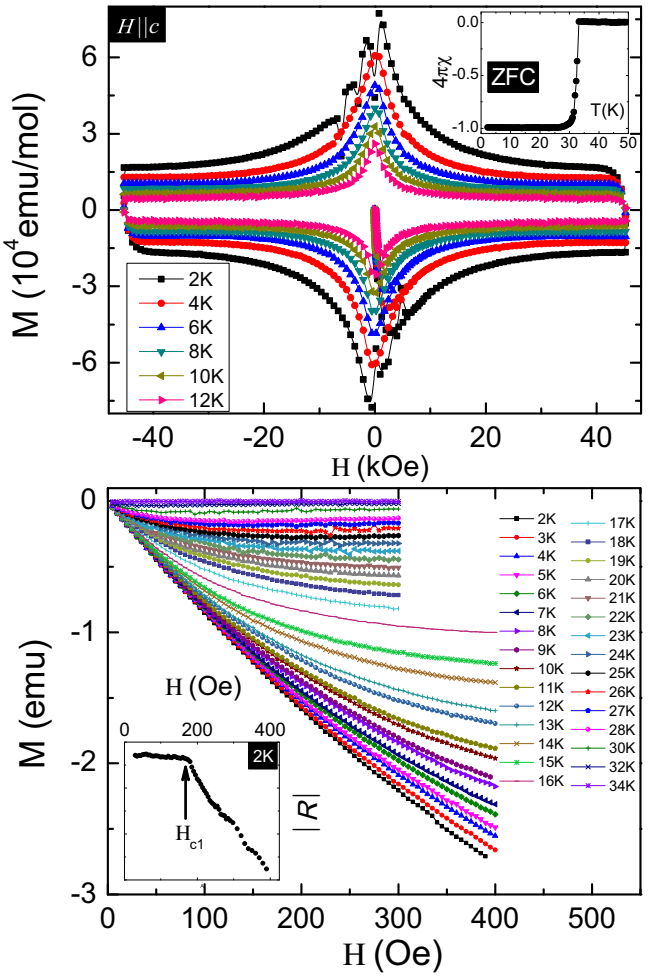

FIG. 1. (Color online) Top: Magnetic-field dependence of the isothermal magnetization M vs H loops measured at different temperatures ranging from 2 to 12 K up to 45 kOe, with the field parallel to the c axis, for a $Ca_{0.32}Na_{0.68}Fe_2As_2$ single crystal. Inset: Temperature dependence of the zero-field-cooled magnetic susceptibility χ after demagnetization correction in an external field of 10 Oe applied along c. Bottom: Initial part of the magnetization curves measured at various temperatures for $H \parallel c$. Inset: An example used to determine the H_{c1} value using the regression factor R at $T = 2$ K.

applied along th c axis. The dc magnetic susceptibility exhibits a superconducting temperature transition with an onset at 34 K. It is worth mentioning that our system exhibits a strong bulk pinning reflected by the symmetric hysteresis loops about the horizontal axis $M = 0$. In addition, the superconducting $M(H)$ exhibits no magnetic background. This indicates that the sample contains negligible magnetic impurities. The virgin $M(H)$ curves at low fields at several temperatures are collected in Fig. 1 (bottom) for $H \parallel c$. In order to determine the transition from linear to nonlinear $M(H)$, a user-independent procedure consisting of calculating the regression coefficient R of a linear fit to the data points collected between 0 and H, as a function of H, is used. Then H_{c1} is taken as the point where the function $R(H)$ starts to deviate from linear dependence. This procedure is similar to that previously used in the studies shown in Refs. [24,50] and illustrated for a particular temperature $T = 2$

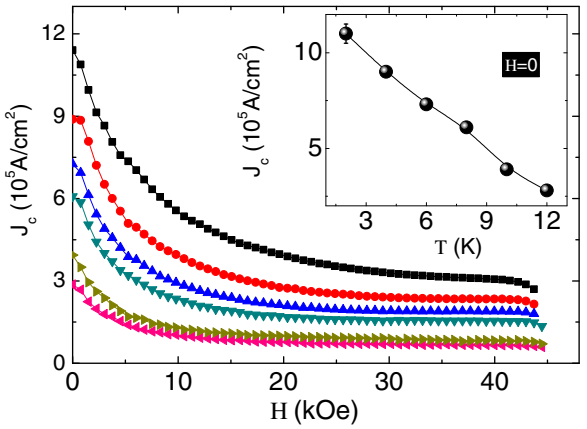

FIG. 2. (Color online) Critical current density J_c at various temperatures up to 45 kOe for $H \parallel c$. Inset: Temperature dependence of the J_c values at $H = 0$ for a $Ca_{0.32}Na_{0.68}Fe_2As_2$ single crystal. The line is a guide for the eyes. The error bar at $T = 2$ K shows the uncertainty of the estimated value due to the irregular jumps close to $H = 0$.

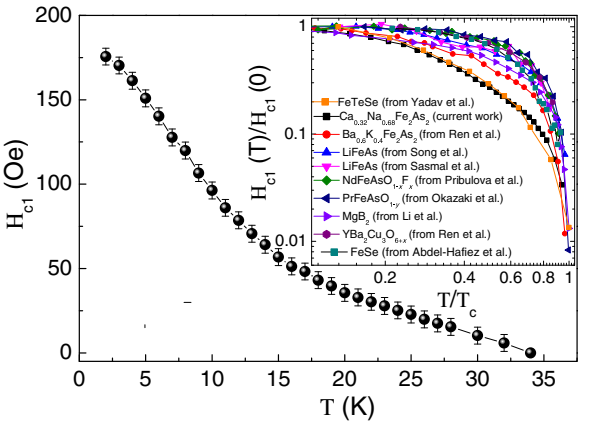

FIG. 3. (Color online) Temperature dependence of H_{c1} vs temperature for a field applied parallel to the c axis. H_{c1} has been estimated from the regression factor (see inset in Fig. 2, bottom). Bars show the uncertainty estimated by the deviating point of the regression fits. Inset: Scaling of the lower critical field values of $Ca_{0.32}Na_{0.68}Fe_2As_2$ together with various Fe-based, MgB_2, and cuprate superconductors (see text).

K in the inset in Fig. 1 (bottom). From the magnetization hysteresis loops $M(H)$, we calculated the critical current density J_c by using the critical state model with the assumption of field-independent J_c. We obtain $J_c \sim 1.15\times10^6$ A/cm^2 for $H \parallel c$ at 2 K (see Fig. 2). The inset in Fig. 2 demonstrates a strong temperature dependence of $J_c(H = 0)$. In addition, the error bar at $T = 2$ K shows the uncertainty of the estimated value due to the irregular jumps close to $H = 0$.

Due to the high sensitivity, the measurements on bulk single crystals will detect first flux line penetration into areas with large demagnetizing fields such as sharp corners, edges, or inclusions of the normal-state defects [51]. In addition, determining H_{c1} from magnetization measurements is not always reliable, since this type of effect can mask completely the predicted sharp drop in the magnetization at H_{c1}. A popular approach to measuring H_{c1} consists of measuring the magnetization M as a function of H and identifying the deviation of the linear Meissner response, which would correspond to the vortex penetration. This technique implicitly relies on the assumption that no surface barriers are present, thus assuring that H_{c1} coincides with the vortex penetration field. The H_{c1} values illustrated in Fig. 3 for $H \parallel c$ show the most intriguing feature, which is the upward trend with negative curvature over the entire temperature range 0–T_c. A similar trend is reported for $Ba_{0.6}K_{0.4}Fe_2As_2$ [22] and $FeTe_{0.6}Se_{0.4}$ [52]. The inset in Fig. 3 shows the normalized temperature dependence, $H_{c1}(T)/H_{c1}(0)$ versus T/T_c, of $Ca_{0.32}Na_{0.68}Fe_2As_2$ together with various systems of Fe-based superconductors [20–22,24,27,52–54], MgB_2 [55], and $YBa_2MgBCu_3O_{6+x}$ [56].

In the London theory, the penetration depth, $\lambda(T) = \lambda(T = 0) + \delta\lambda(T)$, behaves as $\delta\lambda(T) \propto \exp(\frac{-\Delta}{\kappa_B T})$ at low T in the s-wave pairing with a true gap everywhere on the Fermi surface, reflecting superconducting gap Δ. In d-wave pairing with line nodes, $\delta\lambda(T) \propto T$ at low T in the clean limit. This indicates that $H_{c1}(T)$ depends on the pairing symmetry of anisotropic superconductors. In order to shed light on the pairing symmetry in our system, we estimated the penetration depth at low temperatures using the traditional Ginzburg-Landau theory, where H_{c1} is given by [57] $\mu_0 H_{c1}^{\parallel c} = (\phi_0/4\pi\lambda_{ab}^2)\ln\kappa_c$, where ϕ_0 is the magnetic-flux quantum $\phi_0 = h/e^* = 2.07\times10^{-7}$ Oe cm^2 and $\kappa_c = \lambda_{ab}/\xi_{ab}$ is the Ginzburg-Landau parameter. The value of κ was determined from the equation $\frac{2H_{c1}(0)}{H_{c2}(0)} = \frac{\ln\kappa+0.5}{\kappa^2}$. Solving this equation numerically for $Ca_{0.32}Na_{0.68}Fe_2As_2$ using the values $H_{c1}(0)$ and $H_{c2}(0)$, which is taken from C_P data as reported in Ref. [7], we obtained $\kappa_c = 139$. Using this value of κ, we obtained $\lambda(0) = 212(10)$ nm. This value is in close agreement with the values reported for $Ba(Fe_{0.93}C_{0.07})_2As_2$ [$\lambda(0) = 208$ nm] [58], LiFeAs [$\lambda(0) = 198.4$ nm] [21], La-1111 [$\lambda(0) = 245$ nm] [59], and Sm-1111 [$\lambda(0) = 190$ nm] [60].

B. Theoretical fitting of the lower critical field

To date, concerning the pairing symmetry in Fe-based superconductors, the debate is wide open and various scenarios are still under discussion. For instance, different experimental results are divided between these supporting line nodes [61,62] and isotropic as well as anisotropic nodeless gaps [16,17,46,63–69] and two-gap superconductivity [10,11,70]. Taking this into account, the obtained experimental temperature dependence of $\lambda^{-2}(T)$ was analyzed by using the phenomenological α model (see Fig. 4). This model generalizes the temperature dependence of the gap to allow $\alpha = 2\Delta(0)/T_c > 3.53$ (i.e., α values higher than the BCS value), taking into account the behavior of this function in the strong coupling regime. The temperature dependence of each energy gap for this model can be approximated as [71] $\Delta_i(T) = \Delta_i(0)\tanh[1.82(1.018(\frac{T_{ci}}{T} - 1))^{0.51}]$, where $\Delta(0)$ is the maximum gap value at $T = 0$. We fit the temperature dependence of the London penetration depth using the

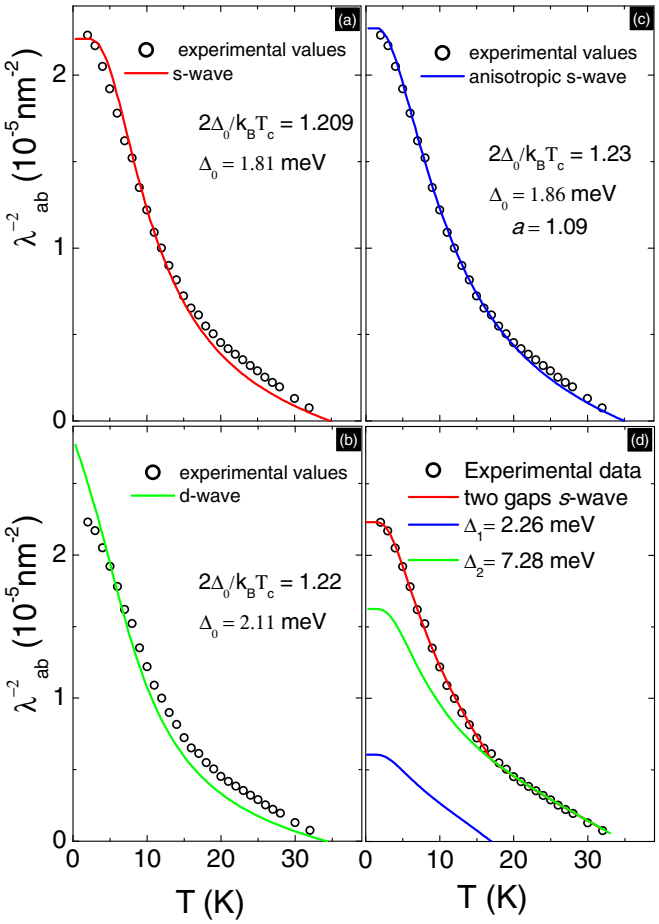

FIG. 4. (Color online) Plots showing the fitting of theoretical curves (by the method described in the text) to experimental data on the temperature dependence of λ_{ab}^{-2} calculated using H_{c1} for a field applied parallel to the c axis. The fits to the experimental data are shown as solid lines for (a) a single s wave (BCS fit), (b) a d wave, (c) an anisotropic s wave, and (d) a two-gap s-wave. Also, in (d), the two solid lines represent the contribution by gaps $\Delta_1(0)$ and $\Delta_2(0)$ to the fitting of λ_{ab}^{-2}.

expression

$$\frac{\lambda_{ab}^{-2}(T)}{\lambda_{ab}^{-2}(0)} = 1 + \frac{1}{\pi}\int_0^{2\pi} 2\int_{\Delta(T,\phi)}^{\infty} \frac{\partial f}{\partial E}\frac{E\,dE\,d\phi}{\sqrt{E^2-\Delta^2(T,\phi)}}, \qquad (2)$$

where f is the Fermi function $[\exp(\beta E+1)]^{-1}$, φ is the angle along the Fermi surface, and $\beta = (k_B T)^{-1}$. The energy of the quasiparticles is given by $E = [\epsilon^2 + \Delta^2(t)]^{0.5}$, with ϵ being the energy of the normal electrons relative to the Fermi level, and where $\Delta(T,\phi)$ is the order parameter as a function of the temperature and angle. For different types of order parameter symmetries (e.g., d wave, anisotropic s wave, etc.), we have different angular dependencies of the order parameter. Thus, the experimental data were analyzed using, for s waves, d waves, and anisotropic s waves, the expressions $\Delta(T,\phi) = \Delta(T)$, $\Delta(T,\phi) = \Delta(T)\cos(2\theta)$, and $\Delta(T,\phi) = \Delta(T)\,(1 + a\cos(\theta))/(1+a)$, respectively, where a is the anisotropy parameter. For the two-gap model, λ_{ab}^{-2} is calculated as [71]

$$\lambda_{ab}^{-2}(T) = r\lambda_1^{-2}(T) + (1-r)\lambda_2^{-2}(T), \qquad (3)$$

where $0 < r < 1$.

The best description of the experimental data for each type of order parameter, single-gap s wave, d wave, and anisotropic s wave and two-gap s wave, is given in Figs. 4(a)–4(d), respectively. The corresponding gap values are shown in these plots. The main features in Fig. 4 can be described as follows: (i) As the first step we compare our data to the single-band s wave and we find a systematic deviation at high-temperature data [see Fig. 4(a)]. (ii) More pronounced deviations exist in the case of the d-wave approach as shown in Fig. 4(b). This clearly indicates that the gap structure of our system is more likely to be nodeless s wave, which compares reasonably well with pervious experimental ARPES data [6]. (iii) Then both the anisotropic s-wave and the two-gap model are further introduced to fit the experimental data. For the anisotropic s wave, the fitting with the magnitude of the gap $\Delta_0 = 1.86$ meV is shown in Fig. 4(c) with an anisotropy parameter $\approx$1.09. As shown, the anisotropic s-wave order parameter presents a good description of the data. (iv) An equally good description of the experimental data for the two-gap s-wave model is obtained using values of $\Delta_1(0) = 2.26$ meV and $\Delta_2(0) = 7.28$ meV. Equations (1) and (2) are used to introduce the two gaps and their appropriate weights. However, we remind the reader that in this approach the one-band expression is generalized to the two-band case. The gap values for each gap are shown individually in Fig. 4(d). It is noteworthy that our extracted gap values are comparable to the two-band s-wave fit, $\Delta_{1,2}(0) = 2.2$ and 8.8 meV, reported for $Ba_{0.6}Ka_{0.4}Fe_2As_2$ [22]. The value of the gap amplitudes obtained for this material scales relatively well with its T_c in light of the recent results for Fe-based superconductors [24,69]. In addition, one can note that the extracted ratio for the anisotropic s-wave order parameter α is smaller than the BCS value, which points to the existence of a large gap.

It is important to note that ARPES studies report two s-wave gaps of 2.3 and 7.8 meV for the outer and the inner Fermi surface sheets, respectively, without any nodes [6]. In fact, ARPES results hint towards the conclusion that the gap value is strongly dependent on the orbital character of the bands forming the corresponding Fermi surfaces: a larger gap appears on d_{xz}/d_{yz} bands [72]. Very recently, and based on a multiband Eliashberg analysis, $Ca_{0.32}Na_{0.68}Fe_2As_2$ demonstrates that the superconducting electronic C_P is well described by a three-band model with an unconventional $s_{\pm}$ pairing symmetry with gap magnitudes of approximately 2.35, 7.48, and -7.50 meV [7]. It has been well demonstrated that the model based on Eliashberg equations is a simplified version of the real four-band model taking into account the similarities between the two 3D Fermi sheets and between the two 2D Fermi sheets. Based on these for the determination of T_c and the gap functions it can be considered that there is a distinct gap only for every 2D and 3D set of bands, respectively [73]. In fact, there are two ways to solve the Eliashberg equations. The first is to solve the equations which contain dependencies of the real frequency, and the second is to solve the equations on an imaginary axis by summing up Matsubara frequencies [74]. In contrast, the α model is not self-consistent, but provides

a popular model with which experimentalists can fit their thermodynamic data that deviate from the BCS predictions and quantify those deviations [75].

Although a clear picture is still missing for the case of $Ca_{0.32}Na_{0.68}Fe_2As_2$, it is important to emphasize that our system could be described via multiband superconductivity. However, from the temperature dependence of the lower critical field data alone it is difficult to be sure whether one, two, or three bands can well describe our investigated system, since in the case of multiband superconductivity low-energy quasiparticle excitations can always be explained by the contribution from an electron group with a small gap.

C. SNS-Andreev spectroscopy

It is widely known that the IMARE develops on cryogenic clefts of some layered superconductors [43]. For example, such SnS-Andreev arrays were found in Gd-1111 [46]. IMARE spectroscopy is a powerful tool to determine bulk superconducting properties, which is why we use this method on $Ba_{0.65}K_{0.35}Fe_2As_2$ single crystals. The current-voltage characteristics, $I(V)$, of the break junctions demonstrate features typical for the SnS-Andreev mode. $I(V)$ for one of these junctions, with excess current at low bias voltages (foot), is shown in Fig. 5 by the solid black line. The foot area in $I(V)$ is manifested in the $dI(V)/dV$ spectrum as a drastic increase in the dynamic conductance. With it, the spectrum reveals a series of peculiarities, shown by n_L labels and arrows, which

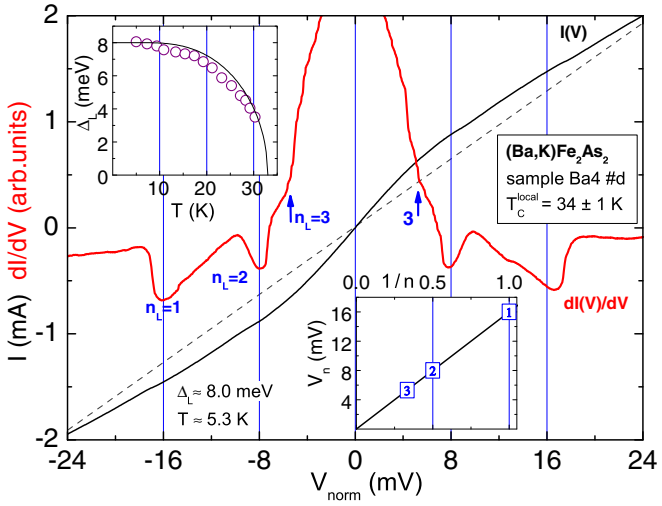

FIG. 5. (Color online) Current-voltage characteristics $I(V)$ and dynamic conductance spectra $dI(V)/dV$ for SNS-Andreev array d realized on a Ba4 sample (two junctions in the stack). The bias voltage is scaled down by a factor of 2, correspondingly. Data were obtained at $T = 5.3$ K. The local critical temperature of the contact point is about 34 ± 1 K. The dashed line is the linear dependence, plotted for comparison. The (blue) n_L labels with arrows indicate the subharmonic gap structure. Upper inset: Experimental $\Delta_L(T)$ data (circles). The solid line is BCS-like dependence. Lower inset: Bias voltages V_n for the n_L series of dips versus their inverse ordinary numbers. Note that the $V_n(1/n)$ dependence (line), as expected, passes through the origin, for $\Delta_L \approx 8.0$ meV.

should form the SGS described by Eq. (1) and corresponds to the theories [34–37]. Although for high-transparent junctions the theory predicts the set of dynamic conductance minima, peculiarity 3 appears to be rather smeared, probably due to the pronounced foot. Such a nontrivial conductance increase may have a multiband nature (several channels of Andreev transport in parallel) and is repeatedly observed in other Fe-based superconductor contacts [46,69]. To check whether the peculiarities form an SGS, we plot the dependence of their positions V_n on the inverse number $1/n$ (see lower inset in Fig. 5). The linear dependence tending to the origin proves that the peculiarities belong to the same SGS. Theory for the MARE by Kümmel *et al.* [37] suggests that the number of visible Andreev minima on dynamic conductance spectra is not less than the l/a ratio. Consequently, for the contact in Fig. 5 one could estimate $l \approx 2a$. The gap magnitude is hence determined as $2\Delta = eV_n n \approx 16.0$ meV. Note that the presence of three peculiarities here increases the accuracy of the gap value obtained. The latter is close to the gap $2\Delta \approx 20$ meV measured in an ARPES study of $Ba_{0.65}K_{0.35}Fe_2As_2$ single crystals from the same batch (see Fig. 1(c) in Ref. [76] for details).

The temperature dependence of this gap, shown in the upper inset in Fig. 5, agrees well with BCS-like behavior (solid line) but curves down slightly. The latter is typical for nonzero interband interaction with another superconducting condensate described by a smaller gap Δ_S (see, for example, [16] and [17]), which is to exist beyond the observed large gap Δ_L. Therefore, the peculiarities observed are caused by the large gap Δ_L. The small gap SGS located at lower biases seemed to be smeared by the foot. The dynamic conductance spectrum becomes flat at approximately 34 K, which corresponds to the termination of Andreev transport, thus defining the local critical temperature T_c^{local} of the contact area. The latter allows us to calculate the BCS ratio $2\Delta_L/k_B T_c^{\text{local}} \approx 5.5$ more exactly. Note that this value is the highest obtained in this work for $Ba_{0.65}K_{0.35}Fe_2As_2$.

Now we detail the shape of Andreev minima in Fig. 5. Bearing in mind the exponential background, one can detect the reproducible shape of $n_L = 1$ and $n_L = 2$ peculiarities. Although the fine structure is smeared, their slight asymmetry suggests that the Δ_L condensate is described by an extended s symmetry. Since the SGS minima are rather pronounced, they have substantial amplitude, and their line shape does not match the theoretically predicted one for the d-wave case [35,38], we conclude there are no nodes in the Δ_L gap. A rough estimation gives about 30% anisotropy in k space. A similar degree of anisotropy could be attributed to gap peculiarities in the spectra presented in Fig. 6.

The $I(V)$ curves in Fig. 6 are rather straight and have less pronounced Andreev peculiarities than those in Fig. 5. It is generally supposed that this suppression of Andreev excess current happens because of the inelastic scattering process at NS interfaces. In our case of $l/a > 1.5$ and atomically flat cryogenic clefts, inelastic scattering should not be a crucial reason for $I(V)$ flattening. A plausible cause is the presence of accidental atoms on the cryogenic clefts, which decreases the contact transparency. If accidental atoms are magnetic (Fe), the magnetic centers could polarize electron spins and, in this way, prevent the electron from finding the pair during the Andreev

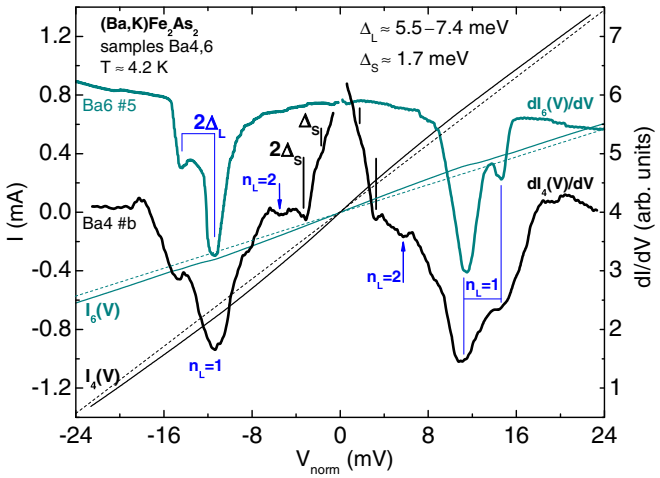

FIG. 6. (Color online) Current-voltage characteristics $I(V)$ (thin) and their dynamic conductance spectra $dI(V)/dV$ (thick lines) for two SNS-Andreev arrays, 5 and b, realized in Ba6 and Ba4 samples from the same batch. Since there are two junctions in the stack, the bias voltage is scaled down by a factor of 2, $T = 4.2$ K. The local critical temperature of the contact point is about 34 ± 3 K. Dashed linear dependencies, crossing the origin, are plotted for comparison. The (blue) n_L labels and arrows indicate the subharmonic gap structure (SGS) of Δ_L; black labels and vertical bars, the SGS of $\Delta_S \approx 1.7 \pm 0.3$ meV. $\Delta_L \approx 5.5$–7.4 meV, the width of the Andreev minima, is determined by the k-space anisotropy of about 30% and represented by the marker lines. Monotonic background of conductance spectra is subtracted.

reflection process. Nevertheless, our experimental setup and the current modulation method we use are sensitive enough to obtain the details of dynamic conductance spectra. The main SGS minima, $n_L = 1$, being rather wide, form doublets caused by the anisotropy of about 25%. The upper curve in Fig. 6 is for the contact obtained in a Ba6 sample and the lower black curve corresponds to a Ba4 sample from the same batch. A smooth background is suppressed here for both spectra. It is easy to see that the fine structure of $n_L = 1$ minima is well reproduced, whereas the current-voltage characteristics presented (thin lines) show considerably different contact resistances and, therefore, contact areas.

The spectra shown in Fig. 6 demonstrate the average value of the large gap $\Delta_L \approx 6.5$ meV, and the resulting BCS ratio $2\Delta_L/k_B T_c^{\text{local}} \approx 4.5$. The anisotropy causes the Δ_L smearing in the range from 5.5 to 7.4 meV. The lower threshold is in good agreement with the minimal value of the hole-band gap from [76]. The lower spectrum, labeled Ba4 #b, has more intensive peculiarities at a low bias. Here, the second Andreev minima, $n_L = 2$, are resolved (marked by arrows). The next minima have a higher amplitude, thus beginning the new SGS. Therefore, the spectrum contains an Andreev structure set by the small gap $\Delta_S \approx 1.7$ meV (marked by vertical bars). Obviously, additional studies are needed for more accurate determination of the small gap.

In the majority of the spectra obtained for $Ba_{0.65}K_{0.35}Fe_2As_2$ we also observed less pronounced peculiarities at bias voltages $V > 2\Delta_L/e$ (not shown here). It is interesting to note that the shape of the lowest spectrum in Fig. 6, for contact b, is similar to that of LiFeAs contact d2 obtained by us earlier (see dashed curve in Fig. 1, Ref. [17], for comparison). Both facts point to the possible presence of a third, and the largest, superconducting gap developing in bands with a vanishing density of states. As for the large gap observed, the BCS ratio $2\Delta_L k_B T_c \approx 5 \pm 0.5$ indicates a strong electron-boson pairing in the Δ_L band.

For the sake of comparison, we have summarized the values of gaps Δ_L, Δ_S, and T_c for $Ba_{0.65}K_{0.35}Fe_2As_2$ extracted from IMARE and for $Ca_{0.32}Na_{0.68}Fe_2As_2$ extracted from magnetization measurements along with other hole-doped 122 materials in Table I. For both investigated systems, the large gap Δ_L has a higher value than the weak coupling BCS ($1.76 k_B T_c$) gap value, which reflects a tendency for strong coupling effects, while the smaller one Δ_S has a value lower than the BCS one. Table I points out that the Δ_L/Δ_S ratio is nearly constant. The mentioned ratio of the systems investigated in this paper is not surprising, being comparable with those of optimally doped $Ba_{0.6}K_{0.4}Fe_2As_2$ [22] and $Ca_{0.32}Na_{0.68}Fe_2As_2$ [7], but disagrees with earlier C_P measurements for a lower-T_c $Ba_{0.65}Na_{0.35}Fe_2As_2$ sample [10]; possible reasons for this inconsistency have been mentioned above. Although the gap values are scattered for different compounds within the 122 family, our obtained gap structure has qualitative similarity to and is comparable with the two-band s-wave fit for the lower critical field data on $Ba_{0.6}K_{0.4}Fe_2As_2$ [22].

A puzzling issue that our results raise is the potential presence of a third gap in the 122 systems. To address this issue and to gain deeper insight into the gap anisotropy, high-precision ARPES or low-temperature STM

TABLE I. Superconducting transition temperature T_c and superconducting gap properties extracted from IMARE and lower critical field (H_{c1}) studies for $Ba_{0.65}K_{0.35}Fe_2As_2$ (three samples) and $Ca_{0.32}Na_{0.68}Fe_2As_2$, respectively, along with 122 other Fe-based superconductors of 122 family.

Compound	T_c (K)	Nodes, anisotropy	Δ_L (meV)	Δ_S (meV)	Δ_L/Δ_S	Technique	Ref.
$Ba_{0.65}K_{0.35}Fe_2As_2$[a]	34 ± 1	No, ≈30%	8–4.8	Invisible	–	Break-junction	This work
$Ba_{0.65}K_{0.35}Fe_2As_2$[b]	34 ± 3	No, ≈25%	7.4–5.5	Invisible	–	Break-junction	This work
$Ba_{0.65}K_{0.35}Fe_2As_2$[c]	34 ± 3	No, ≈25%	7.4–5.7	1.7 ± 0.3	4.35 ± 0.3	Break-junction	This work
$Ca_{0.32}Na_{0.68}Fe_2As_2$	34 ± 1	No	7.28 ± 0.3	2.26 ± 0.3	3.22 ± 0.3	Magnetization	This work
$Ba_{0.6}K_{0.4}Fe_2As_2$	35.8	No	8.9 ± 0.4	2.0 ± 0.3	4.45 ± 0.3	Magnetization	[22]

[a]Sample Ba4, contact d (marked as Ba4 #d in Fig. 5).
[b]Sample Ba4, contact b (marked as Ba4 #b in Fig. 6).
[c]Sample Ba6, contact 5 (marked as Ba6 #5 in Fig. 6).

data would be highly desirable, though they are currently challenging.

D. Conclusions

Using complementary experimental techniques, we have studied single crystals of the 122-FeAs family and obtained consistent data on their superconducting order parameter. From the previous detailed analysis, the temperature dependence of $\lambda_{ab}^{-2}(T)$ is inconsistent with a simple isotropic s-wave type of the order parameter but, rather, favors a two s-wave-like gaps or an anisotropic s-wave order parameter. These observations clearly show that the superconducting energy gap in $Ca_{0.32}Na_{0.68}Fe_2As_2$ is nodeless. In addition, the gaps obtained from our H_{c1} measurements are clearly similar to those determined from ARPES measurements. IMARE spectroscopy of SNS-Andreev arrays formed by the break-junction technique reveals two nodeless gaps: a large gap, $\Delta_L = 6$–8 meV (depending on the small variation of $T_c \approx 34$ K), with extended s-wave symmetry and anisotropy in the k space of not less than ≈30%; and a small gap, $\Delta_S = 1.7 \pm 0.3$ meV. According to our SNS-Andreev data, the BCS ratio for the large gap is $2\Delta_L/k_B T_c \approx 5 \pm 0.5$.

ACKNOWLEDGMENTS

The authors thank Roman Kramer, Anja Wolter-Giraud, Shigeto Hirai, Yaroslav G. Ponomarev, Joris Van de Vondel, Bernd Büchner, and Sabine Wurmehl for fruitful discussions. Our special thank to Sergey Yu. Gavrilkin for the samples characterization. This work was supported by the FNRS projects "Crédit de démarrage U.Lg.," the MP1201 COST Action, and Methusalem Funding of the Flemish Government. We thank the Russian Foundation for Basic Research (Project Nos. 13-02-01180-a, 14-02-90425, and 14-02-92002-a), the Civilian Research Development Foundation (Grant No. FSAX-14-60108-0), (Project No. 73-02-14) for support. Authors also acknowledge the Shared Facility Center at LPI for using their equipment. H.H.W. was supported by NSF of China, the Ministry of Science and Technology of China (973 projects: 2011CBA00102, 2012CB821403, 2010CB923002) and PAPD.

[1] J. Paglione and R. L. Greene, Nat. Phys. **6**, 645 (2010).
[2] A. Chubukov, Annu. Rev. Condens. Matter Phys. **3**, 57 (2012).
[3] H. J. Choi, D. Roundy, H. Sun *et al.*, Nature **418**, 758 (2002).
[4] V. A. Moskalenko, Fiz. Met. Metalloved. **8**, 503 (1959).
[5] H. Suhl, B. T. Matthias, and L. R. Walker, Phys. Rev. Lett. **3**, 552 (1959).
[6] D. V. Evtushinsky, V. B. Zabolotnyy, L. Harnagea, A. N. Yaresko, S. Thirupathaiah, A. A. Kordyuk, J. Maletz, S. Aswartham, S. Wurmehl, E. Rienks, R. Follath, B. Büchner, and S. V. Borisenko, Phys. Rev. B **87**, 094501 (2013).
[7] S. Johnston, M. Abdel-Hafiez, L. Harnagea, V. Grinenko, D. Bombor, Y. Krupskaya, C. Hess, S. Wurmehl, A. U. B. Wolter, B. Büchner, H. Rosner, and S.-L. Drechsler, Phys. Rev. B **89**, 134507 (2014).
[8] D. J. Singh, Phys. Rev. B **78**, 094511 (2008).
[9] D. Kasinathan, A. Ormeci, K. Koch *et al.*, New J. Phys. **11**, 025023 (2009).
[10] A. K. Pramanik, M. Abdel-Hafiez, S. Aswartham, A. U. B. Wolter, S. Wurmehl, V. Kataev, and B. Büchner, Phys. Rev. B **84**, 064525 (2011).
[11] P. Popovich, A. V. Boris, O. V. Dolgov, A. A. Golubov, D. L. Sun, C. T. Lin, R. K. Kremer, and B. Keimer, Phys. Rev. Lett. **105**, 027003 (2010).
[12] F. Hardy, R. Eder, M. Jackson *et al.*, J. Phys. Soc. Jpn. **83**, 014711 (2014).
[13] H. Padamsee, J. E. Neighbor, and C. A. Shifman, J. Low Temp. Phys. **12**, 387 (1973).
[14] S. A. Kuzmichev, T. E. Shanygina, S. N. Tchesnokov, and S. I. Krasnosvobodtsev, Solid State Commun. **152**, 119 (2012).
[15] S. A. Kuzmichev, T. E. Kuzmicheva, and S. N. Tchesnokov, JETP Lett. **99**, 295 (2014).
[16] S. A. Kuzmichev, T. E. Kuzmicheva, A. I. Boltalin, and I. V. Morozov, JETP Lett. **98**, 722 (2014).
[17] T. E. Kuzmicheva, S. A. Kuzmichev, and N. D. Zhigadlo, JETP Lett. **99**, 136 (2014).
[18] T. E. Shanygina, S. A. Kuzmichev, M. G. Mikheev *et al.*, J. Supercond. Nov. Magn. **26**, 2661 (2013).
[19] R. Prozorov and V. G. Kogan, Rep. Prog. Phys. **74**, 124505 (2011).
[20] K. Sasmal, B. Lv, Z. Tang, F. Y. Wei, Y. Y. Xue, A. M. Guloy, and C. W. Chu, Phys. Rev. B **81**, 144512 (2010).
[21] Y. Song, J. Ghim, J. Yoon, K. Lee, M. Jung, H. Ji, J. Shim, and Y. Kwon, Europhys. Lett. **94**, 57008 (2011).
[22] C. Ren, Z.-S. Wang, H.-Q. Luo, H. Yang, L. Shan, and H.-H. Wen, Phys. Rev. Lett. **101**, 257006 (2008).
[23] Anupam, P. L. Paulose, S. Ramakrishnan, and Z. Hossain, J. Phys.: Condens. Matter **23**, 455702 (2011).
[24] M. Abdel-Hafiez, J. Ge, A. N. Vasiliev, D. A. Chareev, J. Van de Vondel, V. V. Moshchalkov, and A. V. Silhanek, Phys. Rev. B **88**, 174512 (2013).
[25] X. L. Wang, S. X. Dou, Z.-A. Ren, W. Yi, Z.-C. Li, Z.-X. Zhao, and S.-I. Lee, J. Phys.: Condens. Matter **21**, 205701 (2009).
[26] C. W. Hicks, T. M. Lippman, M. E. Huber, J. G. Analytis, J. H. Chu, A. S. Erickson, I. R. Fisher, and K. A. Moler, Phys. Rev. Lett. **103**, 127003 (2009).
[27] C. Ren, Z. S. Wang, H. Q. Luo, H. Yang, L. Shan, and H. H. Wen, Physica C **469**, 599 (2009).
[28] L. Harnagea, S. Singh, G. Friemel, N. Leps, D. Bombor, M. Abdel-Hafiez, A. U. B. Wolter, C. Hess, R. Klingeler, G. Behr, S. Wurmehl, and B. Büchner, Phys. Rev. B **83**, 094523 (2011).
[29] L. Shan, Y. L. Wang, B. Shen, B. Zeng, Y. Huang, A. Li, D. Wang, H. Yang, C. Ren, Q. H. Wang, Z. H. Pan, and H. H. Wen, Nat. Phys. **7**, 325 (2010).
[30] H. Q. Luo, Z. S. Wang, H. Yang, P. Cheng, X. Y. Zhu, and H. H. Wen, Supercond. Sci. Technol. **21**, 125014 (2008).
[31] J. Moreland and J. W. Ekin, J. Appl. Phys. **58**, 3888 (1985).
[32] Yu. V. Sharvin, Zh. Eksp. Teor. Fiz. **48**, 984 (1965) [Sov. Phys. JETP **21**, 655 (1965)].
[33] A. F. Andreev, Zh. Eksp. Teor. Fiz. **46**, 1823 (1964) [Sov. Phys. JETP **19**, 1228 (1964)].

[34] G. B. Arnold, J. Low Temp. Phys. **68**, 1 (1987).
[35] T. P. Devereaux and P. Fulde, Phys. Rev. B **47**, 14638 (1993).
[36] M. Octavio, M. Tinkham, G. E. Blonder, and T. M. Klapwijk, Phys. Rev. B **27**, 6739 (1983).
[37] R. Kümmel, U. Gunsenheimer, and R. Nicolsky, Phys. Rev. B **42**, 3992 (1990).
[38] A. Poenicke, J. C. Cuevas, and M. Fogelström, Phys. Rev. B **65**, 220510(R) (2002).
[39] V. N. Zverev, A. V. Korobenko, G. L. Sun, C. T. Lin, and A. V. Boris, JETP Lett. **90**, 130 (2009).
[40] Y. Machida, K. Tomokuni, T. Isono, K. Izawa, Y. Nakajima, and T. Tamegai, J. Phys. Soc. Jpn. **78**, 073705 (2009).
[41] B. Shen, H. Yang, Z.-S. Wang, F. Han, B. Zeng, L. Shan, C. Ren, and H.-H. Wen, Phys. Rev. B **84**, 184512 (2011).
[42] Z.-S. Wang, H.-Q. Luo, C. Ren, and H.-H. Wen, Phys. Rev. B **78**, 140501(R) (2008).
[43] Ya. G. Ponomarev *et al.*, Inst. Phys. Conf. Ser. No. 167, 241 (2000).
[44] B. A. Aminov, L. I. Leonyuk, T. E. Oskina *et al.*, Adv. Supercond. **V**, 1037 (1993).
[45] E. van Heumen, J. Vuorinen, K. Koepernik *et al.*, Phys. Rev. Lett. **106**, 027002 (2011).
[46] T. E. Kuzmicheva, S. A. Kuzmichev, M. G. Mikheev *et al.*, Europhys. Lett. **102**, 67006 (2013).
[47] A. K. Pramanik, L. Harnagea, C. Nacke, A. U. B. Wolter, S. Wurmehl, V. Kataev, and B. Büchner, Phys. Rev. B **83**, 094502 (2011).
[48] A. K. Pramanik, S. Aswartham, A. U. B. Wolter, S. Wurmehl, V. Kataev, and B. Büchner, J. Phys.: Condens. Matter **25**, 495701 (2013).
[49] M. E. McHenry *et al.*, Physica C **190**, 403 (1992).
[50] M. Abdel-Hafiez, A. N. Vasiliev, D. A. Chareev, V. V. Moshchalkov, and A. V. Silhanek, Physica C **503**, 143 (2014).
[51] V. V. Moshchalkov, J. Y. Henry, C. Marin, J. Rossat-Mignod, and J. F. Jacquot, Physica C **175**, 407 (1991).
[52] C. S. Yadav and P. L. Paulose, New J. Phys. **11**, 103046 (2009).
[53] Z. Pribulova, T. Klein, J. Kacmarcik, C. Marcenat, M. Konczykowski, S. L. Budko, M. Tillman, and P. C. Canfield, Phys. Rev. B **79**, 020508 (2009).
[54] R. Okazaki, M. Konczykowski, C. J. van der Beek, T. Kato, K. Hashimoto, M. Shimozawa, H. Shishido, M. Yamashita, M. Ishikado, H. Kito, A. Iyo, H. Eisaki, S. Shamoto, T. Shibauchi, and Y. Matsuda, Phys. Rev. B **79**, 064520 (2009).
[55] S. L. Li, H. H. Wen, Z. W. Zhao, Y. M. Ni, Z. A. Ren, G. C. Che, H. P. Yang, Z. Y. Liu, and Z. X. Zhao, Phys. Rev. B **64**, 094522 (2001).
[56] R. Liang, D. A. Bonn, W. N. Hardy, and D. Broun, Phys. Rev. Lett. **94**, 117001 (2005).
[57] A. L. Fetter and P. C. Hohenberg, in *Superconductivity*, edited by R. D. Parks (Dekker, New York, 1969), Chap. 14.
[58] R. T. Gordon, N. Ni, C. Martin, M. A. Tanatar, M. D. Vannette, H. Kim, G. D. Samolyuk, J. Schmalian, S. Nandi, A. Kreyssig, A. I. Goldman, J. Q. Yan, S. L. Bud'ko, P. C. Canfield, and R. Prozorov, Phys. Rev. Lett. **102**, 127004 (2009).
[59] H. Luetkens, H.-H. Klauss, R. Khasanov, A. Amato, R. Klingeler, I. Hellmann, N. Leps, A. Kondrat, C. Hess, A. Kohler, G. Behr, J. Werner, and B. Büchner, Phys. Rev. Lett. **101**, 097009 (2008).
[60] A. J. Drew, F. L. Pratt, T. Lancaster, S. J. Blundell, P. J. Baker, R. H. Liu, G. Wu, X. H. Chen, I. Watanabe, V. K. Malik, A. Dubroka, K. W. Kim, M. Rossle, and C. Bernhard, Phys. Rev. Lett. **101**, 097010 (2008).
[61] M. Abdel-Hafiez *et al.*, Phys. Rev. B **87**, 180507(R) (2013).
[62] J. S. Kim, B. D. Faeth, Y. Wang, P. J. Hirschfeld, G. R. Stewart, K. Gofryk, F. Ronning, A. S. Sefat, K. Y. Choi, and K. H. Kim, Phys. Rev. B **86**, 014513 (2012).
[63] N. Xu *et al.*, Phys. Rev. B **87**, 094513 (2013).
[64] H. Miao *et al.*, Phys. Rev. B **85**, 094506 (2012).
[65] K. Hashimoto, T. Shibauchi, T. Kato, K. Ikada, R. Okazaki, H. Shishido, M. Ishikado, H. Kito, A. Iyo, H. Eisaki, S. Shamoto, and Y. Matsuda, Phys. Rev. Lett. **102**, 017002 (2009).
[66] Q. Q. Ge, Z. R. Ye, M. Xu, Y. Zhang, J. Jiang, B. P. Xie, Y. Song, C. L. Zhang, P. Dai, and D. L. Feng, Phys. Rev. X **3**, 011020 (2013).
[67] M. P. Allan, A. W. Rost, A. P. Mackenzie, Y. Xie, J. C. Davis, K. Kihou, C. H. Lee, A. Iyo, H. Eisaki, and T.-M. Chuang, Science **336**, 563 (2012).
[68] T. Kondo, A. F. Santander-Syro, O. Copie, C. Liu, M. E. Tillman, E. D. Mun, J. Schmalian, S. L. Budko, M. A. Tanatar, P. C. Canfield, and A. Kaminski, Phys. Rev. Lett. **101**, 147003 (2008).
[69] Ya. G. Ponomarev, S. A. Kuzmichev, T. E. Kuzmicheva *et al.*, J. Supercond. Novel Magn. **26**, 2867 (2013).
[70] R. Khasanov, D. V. Evtushinsky, A. Amato, H.-H. Klauss, H. Luetkens, Ch. Niedermayer, B. Büchner, G. L. Sun, C. T. Lin, J. T. Park, D. S. Inosov, and V. Hinkov, Phys. Rev. Lett. **102**, 187005 (2009).
[71] A. Carrington and F. Manzano, Physica C **385**, 205 (2003).
[72] A. A. Kordyuk, Low Temp. Phys. **38**, 888 (2012).
[73] O. V. Dolgov, R. K. Kremer, J. Kortus, A. A. Golubov, and S. V. Shulga, Phys. Rev. B **72**, 024504 (2005).
[74] D. J. Scalapino, J. R. Schrieffer, and J. W. Wilkins, Phys. Rev. **148**, 263 (1966).
[75] D. C. Johnston, Supercond. Sci. Technol. **26**, 115011 (2013).
[76] D. V. Evtushinsky, V. B. Zabolotnyy, T. K. Kim *et al.*, Phys. Rev. B **89**, 064514 (2014).